A Quantum Study on the Reaction between C(^{3}P) and Acetylene†

Erasmo Buonomo and David C. Clary*

Department of Chemistry, University College London, 20 Gordon Street, London, WC1H 0AJ, U.K.

Received: October 18, 2000; In Final Form: January 18, 2001

The reaction between carbon atoms (C(^{3}P)) and acetylene has been studied by a reduced dimensionality approach, restricted to the initial addition channels, in the energy range between 5 and 70 kJ mol^{-1}. Coupled cluster calculations with single and double substitution and a non iterative estimate of the triple excitation (CCSD(T)) have been used to generate the lowest triplet potential energy surface. The flux into two different reaction channels, leading to linear and cyclic isomers of C_3H, has been calculated by solving the time dependent Schrödinger equation. Results show that linear C_3H is preferentially formed, while cyclic C_3H is formed only at the highest energy of the calculations. Furthermore, the adiabatic capture-coupled states approximation (ACCSA) has been employed to generate rate constants at low temperatures, using the CCSD(T) potential, giving an improvement on the results obtained by using the long-range part of the potential.

1. Introduction

The importance of fast neutral−neutral reactions, involving at least one radical, has been recognized in the study of the evolution of the dense interstellar clouds (ISC).[1−3]. In the region of the dense ISCs where molecules exist,[2−4] the density is extremely low (about 10−10000 molecule/cm^{-3}), so that three body collision are ruled out. These regions are also very cold, with typical temperatures in the range of 10−50 K. Therefore, only exothermic reactions without an entrance barrier can contribute to the chemistry of the dense ISCs.

Recently, the relevance of neutral−neutral reactions has been pointed out by rate constant measurements[5] on the reaction between carbon atoms and unsaturated hydrocarbons, reporting very high values of the rate constant at room temperature. Low-temperature measurements (down to 15K) of the rate constants for reaction involving several radicals (including C, OH, CN, and CN)[6,7] have been done, showing that these reactions remain very rapid even at such low temperature, sometimes with an increase of the rate constants with decreasing temperature. Such studies have prompted the inclusions of rapid neutral−neutral reactions in the networks used by astrophysicists in modeling the evolution of dense ISCs,[1,8] showing marked effects on the calculated abundancies of some species. In general, these reactions have smaller rate constants than those for ion−molecule reactions, usually taken as responsible for the chemistry of ISCs. However, fast neutral−neutral reactions provide more direct ways to obtain some complex molecules, for which several ion−molecule reaction steps would be required. The importance of neutral−neutral reactions is also enhanced by the fact that neutral particles are more abundant than the corresponding ions.

Rate constants measurements[5,9] have shown that the reaction between carbon atoms (C(^{3}P)) and unsaturated hydrocarbons are fast and therefore can be important in the chemistry of dense ISCs, in particular as a way to synthesize long chain linear hydrocarbons.[10] Since kinetic measurements are carried out by monitoring the disappearance of the reagents, alternative experiments are needed to identify the products, expecially in the case of neutral reactions for which, usually, several reaction channels are possible. Recently molecular beam studies[11,12] on C(^{3}P) reactions have been undertaken, providing a direct identification of the products of the reactions. The reactive channels corresponding to the elimination of a hydrogen atom have been investigated, in the energy range of the order of 10^{3}K. Even if the energies are too high to be directly relevant to the chemistry of the ICSs, those experiments have revealed new information on the dynamics of this class of reactions. The experimental results, together with high level ab initio calculations,[13,14] have revealed that many reactive routes are accessible even at very low energies. Stable addition intermediates are involved in those reactive routes, for which the isomerization processes are often possible. Furthermore, since radicals are involved, more than one potential energy surface has to be taken into account to explain the dynamics of those reactions.

One of the most studied reactions in this class is that between C(^{3}P) and acetylene, that was found to be very fast at room temperature.[5] In addition, low-temperature measurements have been performed recently, showing that the rate constant has a very slight negative dependence on the temperature.[9] These experimental rate constants show a reasonable agreement with theoretical estimates based on capture theory approximations,[5] pointing out that the frequency of a reactive event is almost the same as the collision frequency. Molecular beams studies[11] have observed C_3H as a product of the reaction. Since two different isomers of C_3H, linear and cyclic, have been observed in different ISCs, the reaction provides a direct way to synthesize them efficiently.[11] Molecular beam experiments at very high energy[15] (≈200 kJ mol^{-1}) have reported the formation of CH as a product, corresponding to an endothermic channel. Even if this study is not relevant for the chemistry of the ICSs, the results emphasize how all the reaction paths accessible at a given energy cannot be neglected without a detailed dynamical study. Quantum calculations of rate constants[16] have been done by using different methods. Approximate methods, based on capture theory, have been used to calculate rate constants at low temperature, showing a partial agreement with the experimental results, with a better agreement at lower temperature. The authors[16] have pointed out the inaccuracy of a description of

† Part of the special issue "William H. Miller Festschrift".

10.1021/jp003837p CCC: $20.00
Published on Web 02/24/2001

the neutral−neutral reactions based on the long range part of the potential, which has been successfully applied to ion−molecule reactions. In a different range of temperature (300−1000 K), relevant for combustion processes, variational Rice−Ramsberger−Kassel−Marcus (RRKM) calculations[17] have been performed on the present system, starting from very accurate ab initio calculations of the stationary points of the lowest triplet surface. The results are in rather good agreement with the high tail of the experimental results.[9] Those calculations have identified the bottleneck of the reaction in the addition step.

The aim of the present study on the reaction between a carbon atom (^{3}P) and acetylene is 2-fold: to calculate reactive cross sections and branching ratios for the formation of the linear and cyclic C_3H, in the energy range of the molecular beam experiments[11] and to produce rate constants at low temperature from an accurate ab initio potential. As we have discussed before, such reactions are quite challenging from the theoretical point of view. In the following section, we describe the model we have introduced to reduce the complexity of the calculations. In section 3, we discuss the calculation of the accurate ab initio potential energy surface used in the dynamical calculation. The implementation of the dynamical models used is this work is described in section 4. The results are reported in section 5, followed by section 6 where some conclusions about the findings of the present work are drawn.

2. Dynamics and Modelling of the Reaction

As we have discussed before, the reaction

$$C(^3P) + C_2H_2 \rightarrow C_3H + H \qquad (1)$$

has been the subject of molecular beams experiments by Kaiser et al.,[11] at collision energies in the range between 8.8 and 45 kJ mol^{-1}. The center-of-mass angular distribution of the observed products of the reaction, C_3H, shows forward scattering at the lowest energies while is isotropic at 45 kJ mol^{-1}; the translational energy distributions are peaked toward zero, and are extended up to energies that are ≈10 kJ mol^{-1} larger than the collision energies. The ratio of the observed scattered intensities shows a decrease of the cross sections with energy consistent with the behavior predicted by a capture theory approximation.[5]

The translational energy distributions seem to indicate that the H atom leaves the collision complex on an almost barrierless reaction path, giving a product C_3H with a very small exothermicity while the angular distributions are not consistent with the formation of a long-lived collision complex. From the kinematics of the reaction, ab initio calculations[13] and comparisons with other related systems, the authors[11] have rationalized the experimental results with the hypothesis of the competition between two microchannels, one leading to forward scattering (mechanism (a)) while the other gives the symmetrical angular distribution (mechanism (b)). Mechanism (a) consists of the addition of the incoming carbon to the molecule to form cyclopropenylidene (c-C_3H_2), followed by the C−H fission leading to the cyclic C_3H. In the other mechanism, (b), the addition of the carbon atom forms a bent C_3H_2 (*S*-trans-propenediylidene), which undergoes a fast 2,3-hydrogen shift to give the linear C_3H_2 (propargylene), finally leading to linear C_3H. Mechanism (a) is direct and is quenched at higher collision energy, while mechanism (b) acts on a shorter time scale than the rotational period of the complex and justifies the isotropic distribution of the products with the symmetry of the linear intermediate (l-C_3H_2). Both mechanisms only involve the lowest triplet surface of C_3H_2, thus excluding the lowest singlet surface and two excited triplet surfaces (asymptotically correlated with the triplet ground state) also accessible in the same energy range. Ab initio calculations by Ochsenfeld et al.,[13] at the coupled cluster CCSD(T)) level, have reported relative energies of −8.6 kJ mol^{-1} for the cyclic C_3H and −1.5 kJ mol^{-1} for the linear C_3H with respect to the energy of the reagents, while other calculations (MultiReference CI,[18] CASSCF//ICCI[17]) have given a small endothermicity for the formation of the two products, (4−8 kJ mol^{-1}). The absence of a barrier for the C−H fission has been verified by CASSCF//ICCI[17] calculations, from all the C_3H_2 isomers.

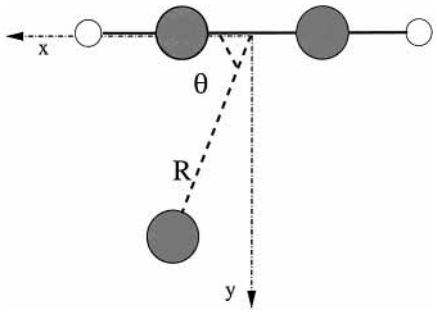

Figure 1. Polar and Cartesian coordinates used in the study of the addition of carbon to C_2H_2. The origin is placed at the C−C midbond of acetylene

From the above description of the reaction, the outcome of the collision will be determined by the formation of the addition adduct, C_3H_2, on the triplet surface.

Given the number of degrees of freedom, it is extremely difficult to attempt a complete theoretical study of this system. Some approximations are needed to reduce the problem to a complexity that can be managed with the current computational and theoretical resources. The findings of the molecular beams experiments reported above[11] can be a starting point to formulate a model for the description of the reaction. Therefore, it is reasonable to assume that the reaction takes place on the ground triplet surface. It is also assumed that the addition step, leading to the intermediate C_3H_2, determines which product will be formed according to the following scheme:

$$C + C_2H_2 \rightarrow (c\text{-}C_3H_2) \rightarrow H + \text{cyclic } C_3H \qquad \text{(mechanism (a))}$$

$$C + C_2H_2 \rightarrow (l\text{-}C_3H_2) \rightarrow H + \text{linear } C_3H \qquad \text{(mechanism (b))}$$

and that the reaction is direct, i.e., the reaction time is of the order of the collision time. The final assumption is that the addition process can described by two coordinates giving the position of the incoming carbon atom with respect to acetylene (Figure 1). Thus, the process will be considered vibrationally adiabatic with respect to all the remaining degrees of freedom (corresponding to the internal modes of the acetylene molecule). The approximations introduced allow us to study the reaction by considering only the entrance channel, up to the formation of the C_3H_2 intermediates. The redistribution of the excess energy into the other modes, including the C−H dissociative mode, will not be taken into account since they can be reasonably treated adiabatically in the addition step.

The model, therefore, provides an estimate of the cross section for the formation of both the linear and cyclic C_3H isomers. The total cross section will be also calculated: in this case the accuracy will not depend on the assumptions of the model but rather on the accuracy of the potential energy surface employed.

3. C_3H_2 Potential Energy Surface

The C_3H_2 potential energy surface has three important isomers (cyclopropenylidene, c-C_3H_2; propargylene, l-C_3H_2; and vinylidenecarbene, H_2CCC) which have been the subject of several experimental and theoretical studies, where different properties of those structures have been investigated (see refs 19 and 20 for a review).

Ab initio calculations have show that the two isomers cyclopropenylidene (c-C_3H_2)[18,21,22] and vinyldenecarbene[21,22] have their most stable structures on the singlet surface, while propargylene (l-C_3H_2) has its most stable form on the lowest triplet surface.[18,20−23] The most stable isomer is cyclopropenylidene. However, photolysis studies of C_3H_2[19,24] have shown that the isomerizations among all the above structures are possible, even at relatively small photon energies. This process might also be involved in the photodissociation of propyne (CH_3CCH) where the product C_3 has the same rotational distribution that has been observed in photodissociation of allene (H_2CCCH_2):[25] C_3H_2 is a product of the primary dissociation of the two C_3H_4 isomers and one of its isomers can be the common intermediate that can justify these results. In the context of this work, it is worth mentioning that in the photolysis experiment,[19] propargylene (l-C_3H_2) is not converted into the other two isomers at the lowest photon energies used in the experiments (<260 kJ mol^{-1}), thus giving a lower estimate for the energy required for the transition from the triplet surface to the lowest singlet surface. A recent ab initio calculation[20] has treated the problem of the isomerizations among the most stable C_3H_2 structures, using high level configuration interaction methods. The energies of the transition states on the singlet PES and the minima on the seam of crossing (MSX) between the singlet and the triplet PES reported in this work seems to indicate that all the isomerizations are energetically allowed for the reaction between C(^{3}P) and acetylene.

The reaction between C(^{3}P) and acetylene, on the lowest triplet surface, has been studied recently using different configuration interaction methods: these include Möller−Plesset perturbation theory[18] calculations, in which the lowest singlet state has also been taken into account, coupled cluster with single and double excitation and a non iterative correction of the triple excitation (CCSD(T)),[13] where minima on the triplet surfaces have been determined and complete active space self-consistent field (CASSCF)[17] calculations, in which reaction paths for (1) have been reported. Minima on the triplet surface have also been determined by a density functional study of reaction between CH and acetylene.[22] In the present study, the task is to calculate the interaction for the addition of a carbon atom to acetylene, as a function of the distance and orientation of the carbon atom with respect to acetylene (see Figure 1) and then use the reduced dimensionality potential energy surface for dynamical calculations.

In the next sections, the results obtained by ab initio calculations and the interpolation to generate a PES appropriate for scattering calculations are described.

3.1. Ab Initio Calculations. Electronic structure calculation in this section have been carried out using the coupled cluster theory with single and double excitations and a noniterative contributions of triple excitations (CCSD(T)). The Gaussian98[26] set of programs has been used to carry out calculations of geometry optimizations (minima and saddle points) and frequency calculations, in order to classify stationary points and evaluate zero point energies (z.p.e), using the CCSD(T) implementation.[27] CCSD(T) calculations have already been done on this system and the method is able to correct the spin contamination of the UHF solution that affects other quantum chemistry methods.[13,23] The energies of stationary points reported below include the contribution of zero point energies in the harmonic approximation; the zero of the energy scale is defined at the energy of the reagents (corrected for the z.p.e). The basis set used is the correlation consistent polarized valence double-ζ (cc-pVDZ) basis.[28]

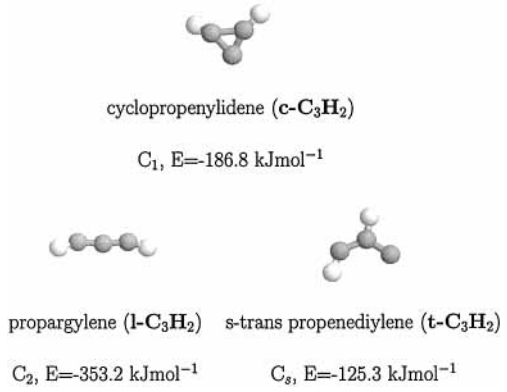

Figure 2. C_3H_2 minima, obtained by CCSD(T)/cc-pVDZ calculations.

The minima of the lowest triplet state of C_3H_2 that are relevant to this study are shown in Figure 2. Cyclopropenylidene (c-C_3H_2) has no symmetry (C_1) and an energy of −186.8 kJ mol^{-1} with respect to the reagents, in good agreement with other values reported in the literature (−213.0[13] and −189.5 kJ mol^{-1} [17]). Geometries are very close (i.e., bond distances within 0.01 Å and bond angles within 1°) to those found previously,[13,17,18] with the exception of C−H bonds that are larger by less than 0.02 Å; frequencies are very close to those found in previous CCSD(T) calculations,[13] using a triple-ζ polarization basis set.

Propargylene (l-C_3H_2) is the most stable isomer on the triplet surface, with an energy of −353.2 kJ mol^{-1} (to be compared with −385.4[13] and −351.0[17]). The geometry has C_2 symmetry, in agreement with experiments[29] and ab initio calculations at different level of theory, from DFT[20] to CCSD(T)[13,20] and quadratic configuration interaction with single and double excitations and perturbational treatment of triple excitations (QISD(T)).[23] Bond lengths and angles obtained in this study are in good agreement with the QISD(T) calculations.[23] Other calculations report C_s geometries,[17,18] but the energy difference between the two geometries is very low because of the nonrigidity of propargylene. The lowest frequency found in this study is 248 cm^{-1} (incidentally very close to the experimental value, 249 cm^{-1} [19]), clearly showing this feature of the molecule. Other frequencies agree rather well with those found previously with CCSD(T) methods.[13]

The last structure reported in Figure 2, *S*-trans-propenediylidene (*t*-C_3H_2), has C_s symmetry and an energy of −125.2 kJ mol^{-1} (compared to −134.6[13] and −121.3[17]). Reaction path calculations[17] have shown that *t*-C_3H_2 is the common intermediate along the path leading to c-C_3H_2 and l-C_3H_2. Despite a very low frequency, geometrical parameters agree very well with earlier results, in particular with CCSD(T) calculations.[13] Frequencies found in this calculations are similar to those reported in previous CCSD(T)[13] calculations.

Two saddle points, probably the most important in the addition process on the triplet surface, have been localized by geometry optimization and are shown in Figure 3. Geometries and frequencies are reported in Table 1. The first saddle point, sp1, separates c-C_3H_2 from the linear C_3H_2; its energy is −131.9 kJ mol^{-1} with respect to the reagents, 54.7 kJ mol^{-1} higher than c-C_3H_2. The energy value much lower than zero clearly

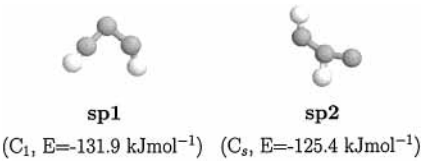

Figure 3. Saddle points for the insertion path (sp1) and the hydrogen transfer process (sp2), obtained from CCSD(T)/cc-pVDZ calculations.

TABLE 1: Geometries and Frequencies (cm^{-1}) of the Saddle Points for the Insertion Path (sp1) and Hydrogen Transfer Path (sp2), Calculated by Using the CCSD(T) Method.

	geometry	frequencies/cm^{-1}
sp1	r(H1−C1) = 1.085 Å	253.3 337.4
	r(H2−C3) = 1.099 Å	
	r(C1−C2) = 1.296 Å	743.3 792.1
	r(C2−C3) = 1.439 Å	
	α(H1−C1−C2) = 178.5°	1087.0 1626.5
	α(H2−C3−C2) = 139.0°	
	α(C1−C2−C3) = 92.9°	3201.1 3381.9
	ϕ(H1−C1−C2−C3) = −168.8°	
	ϕ(H2−C3−C2−C1) = 35.7°	705.1i
sp2	r(H1−C1) = 1.142 Å	405.8 533.5
	r(H2−C3) = 1.094 Å	
	r(C1−C2) = 1.347 Å	745.5 961.5
	r(C1−C3) = 1.395 Å	
	α(H1−C1−C3) = 121.1°	1106.2 1527.5
	α(H2−C3−C1) = 132.6°	
	α(C2−C1−C3) = 151.0°	2825.4 3262.0
		184.6i

shows that the insertion of the (^{3}P) atom into the triple bond of acetylene is energetically allowed at any collision energy. This result has already been reported in CASSCF calculations,[17] where the saddle point for the ring opening has been found with energy of −130.5 kJ mol^{-1} (59.0 kJ mol^{-1} from c-C_3H_2) and a geometry quite similar to the one obtained in the present study, apart from a marked difference in one dihedral angle (ϕ (H2−C3−C2−C1) = 83.1°[17] compared with ϕ (H2−C3−C2−C1) = 35.7°). Frequencies are also in general agreement, with two exceptions (559 and 944 cm^{-1} [17] instead of 743 and 792 cm^{-1}) The second saddle point, sp2, is the transition state for the 1−2 hydrogen transfer, connecting t-C_3H_2 with the linear isomer. The energy is −125.4 kJ mol^{-1}, just 0.1 kJ mol^{-1} higher that t-C_3H_2: the result indicates that this process should be very fast. Previous CASSCF results have given an energy of −111.3 kJ mol^{-1}, giving a barrier of 10 kJ mol^{-1} with respect to t−C_3H_2. Geometries differ by less than 0.02 Å in bond distances and a few degrees in bond angles (the larger disagreement is 5.1°, found for α(C1−C2−C3)). Frequencies are also very close, apart from the imaginary frequency (395 cm^{-1} [13] compared to 185 cm^{-1})

Figure 4 shows the energy diagram for the addition process. Energies of the products are taken from ref 13 and have been reported to underline the relation between exit channels and C_3H_2 intermediates formed in the addition process, together with the lack of exit barriers. The simplified picture shown in the diagram only reports what could be considered as the most important intermediates and saddle points in the reaction of carbon (^{3}P) to acetylene on the lowest triplet surface. Another intermediate (not taken into account in this study), vinyldene-carbene (H_2CCCH), has been found along another pathway that leads to linear C_3H. However, CASSCF calculations[17] have found a saddle point with a rather high energy (−40 kJ mol^{-1}) along the path for the formation of H_2CCC. The path is accessible at any energy but its contribution should be less important considering the wide range of impact parameters involved in the reaction and the small impact parameter required to reach this saddle point (≈ 2 Å[17]). On the other hand, Figure 4 reports more straightforward paths for the formation of linear C_3H, passing through the linear intermediate l-C_3H_2.

A potential energy surface for the addition process has been calculated as a function of the coordinates R and θ, describing distance and orientation of the approaching carbon atom with respect to acetylene (Figure 1): the origin of the coordinate system is placed in the C−C mid bond of acetylene. The other seven degrees of freedom have been optimized. The partially spin restricted coupled cluster method (RCCSD(T)),[30,31] implemented in the quantum chemistry package Molpro,[32] has been employed, with the cc-pVDZ[28] basis set. Ab initio calculations showed that the optimization at small values of θ could be restricted to C_s geometries, thus saving two degrees of freedom in the optimization, while for larger values of the angle ($\theta \geq 45°$) all the implicit degrees of freedom have to be optimized (C_1 geometries), since, for instance, the energy difference between c-C_3H_2(C_s) and c-C_3H_2(C_1) is larger than 20 kJ mol^{-1}. The grid is composed of 14 angles, chosen according to the features of the surface, for which a variable number of points, between 25 and 50, have been calculated. Zero point energies have not been included, as it would have been too demanding in computational resources; however, their effect on the interaction energies can be considered negligible. Estimates on the stationary points described above give an error on the interaction energies smaller than 10 kJ mol^{-1}.

The short-range part of the potential, obtained from the fitting procedure described in the following section, is shown in Figure 5. The figure reports the interaction energy between carbon and acetylene as a function of the position of the carbon atom with respect to the acetylene C−C mid bond. The surface has a quite complicated topology, there are other minima and saddle points apart from those reported in Figure 4. Two paths for the reaction are visible on the figure. The first path, along $x = 0$ Å, passes through c-C_3H_2 (its well is located around $x = 0.2$ Å, $y = 1.1$ Å) and reaches l-C_3H_2 (around $x = 0$ Å, $y = 0.2$ Å) after passing the ring opening saddle point. This describes the insertion of the carbon atom in the acetylene triple bond. The second path, duplicated by symmetry, leads to l-C_3H_2 (at $x = 2$ Å, $y = 0.2$ Å) after passing t-C_3H_2 (shallow well around $x = 1.5$ Å, $y = 1.1$ Å) and the saddle point for the hydrogen tranfer. The scheme of Figure 4 is therefore included in the surface, but the dynamics will be strongly dependent on all the features on the surface before reaching the two valleys.

The surface has been extended in the asymptotic region by the following long-range interaction potential:[16,33]

$$V_{\text{asym}}(R,\theta) - \frac{C_6}{R^6}[1 + \Delta_1 + 2\Delta_1 P_2(\cos\theta)] \qquad (2)$$

where the coefficients C_6 and Δ_1 can be expressed in term of polarizabilities and ionization potentials of C and C_2H_2. The values used are $C_6 = 43.05$ eV Å^6 and $\Delta_1 = 0.156$[16] The matching between the *ab initio potential* and the asymptotic interaction (eq 2) has been done using the matching function[34]

$$f_{\text{match}}(R) = \begin{cases} 1 & R < R^* \\ \exp(-(R - R^*)^2/2\sigma^2) & R \geq R^* \end{cases} \qquad (3)$$

and the potential is given by

$$V(R,\theta) = V_{\text{asym}}(R,\theta) + f_{\text{match}}(R) * (V_{\text{calc}}(R,\theta) - V_{\text{asym}}(R,\theta)) \qquad (4)$$

where V_{calc} is the fit of the ab inito potential. The function f_{match} guarantees the continuity of potential and its first derivative.

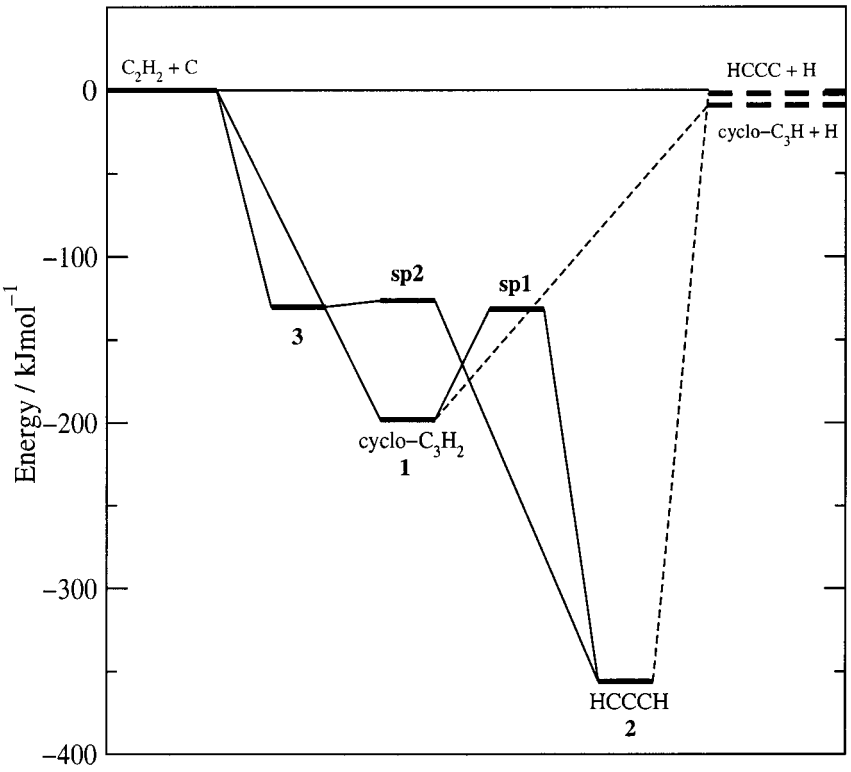

Figure 4. Energy diagram for reaction 1 obtained in this work: energies of the product (dashed lines) are taken from ref 13.

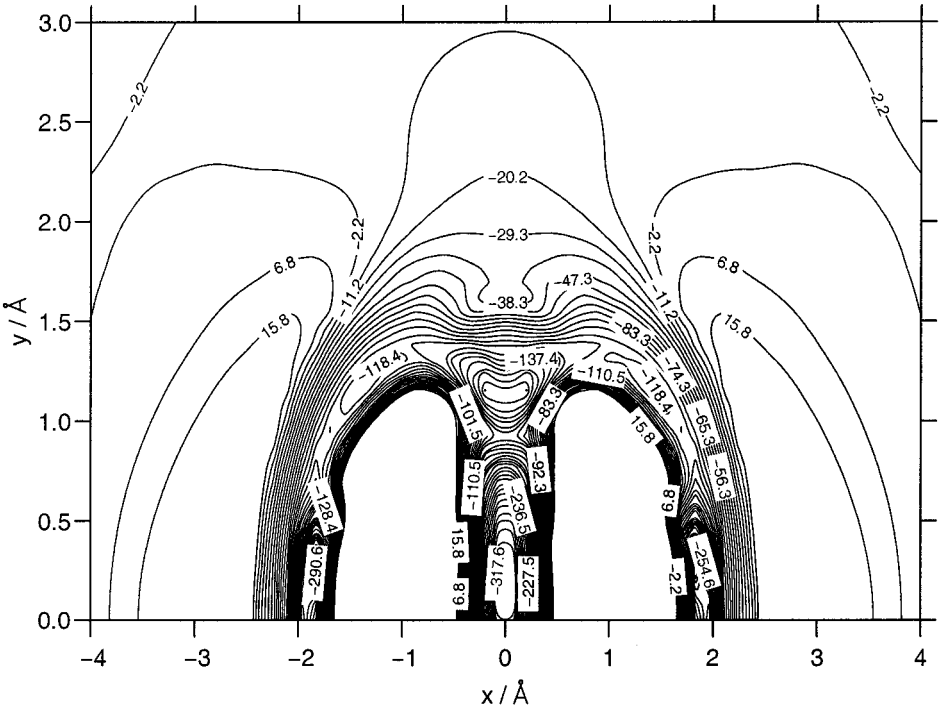

Figure 5. Potential energy surface (interaction region) as a function of Cartesian coordinates (see Figure 1). Contour levels in kJ mol^{-1}, distances in angstroms.

The value of σ, independent from the angle θ, has been determined from the condition of switching to the asymptotic form at $R = 9$ Å and the starting point of the function has been chosen at $R^* = 6$ Å.

3.2. Potential Fitting. A numerical representation of the PES has been obtained using the distributed approximating functional (DAF) method,[35,36] which is able to produce a smooth and accurate fit of the input points. This method generates a local fit of the surface, V_{app} for each point **R** for which the potential is evaluated

$$V_{app}(\mathbf{R}';\mathbf{R}) = \sum_j a_j(\mathbf{R})\phi_j(\mathbf{R}';\mathbf{R}) \qquad (5)$$

where $\{\phi_j\}$ is a truncated basis set centered on **R** and $\{a_j\}$ are the expansion coefficients, to be determined from the least-squares condition in which a non negative weight function for the input data, centered on **R**, is introduced. Alternatively, it is

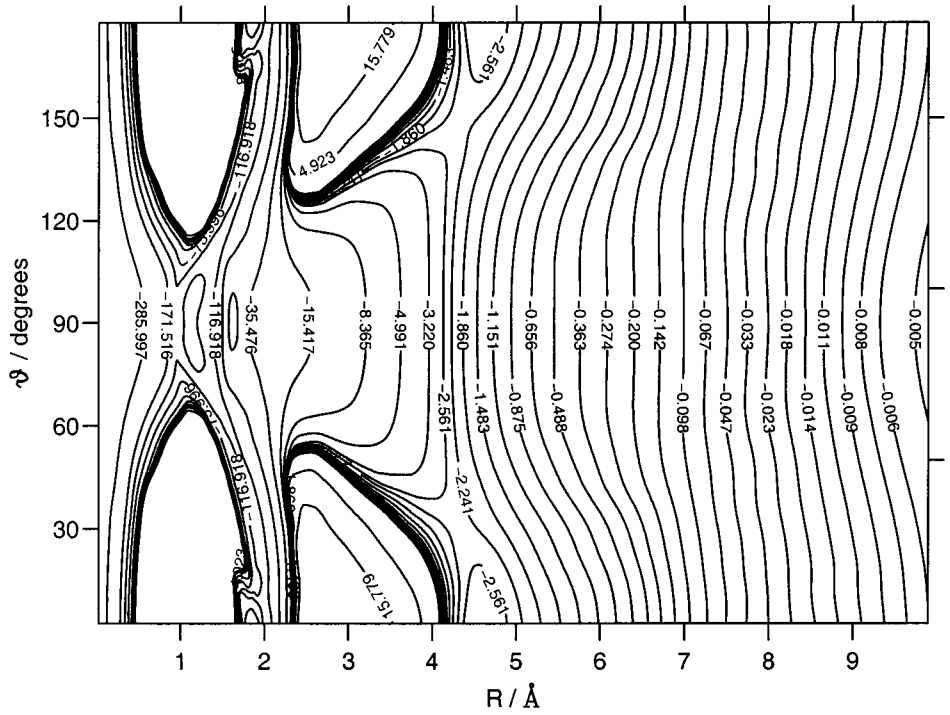

Figure 6. Potential energy surface as a function of polar coordinates (Figure 1). Contour levels in kJ mol^{-1}, distances in angstroms, angles in degrees.

possible to define an inner product on the grid

$$\langle \xi | \eta \rangle = \sum_{\text{grid}} w(\mathbf{R}';\mathbf{R}) \xi^*(\mathbf{R}';\mathbf{R}) \eta(\mathbf{R}';\mathbf{R}) \tag{6}$$

and if the basis set is orthonormal with respect to the inner product, the coefficients $\{a_j(\mathbf{R})\}$ take the simple form

$$a_j(\mathbf{R}) = \langle V_{\text{grid}} | \phi_j \rangle \tag{7}$$

where V_{grid} is the set of input points. The value of the DAF fit on the point $\mathbf{R}$ is given by

$$V_{\text{DAF}}(\mathbf{R}) = V_{\text{app}}(\mathbf{R};\mathbf{R}) \tag{8}$$

This procedure is repeated for all the points to be fitted.

In this work, the DAF fit has been generated as in ref 36: a basis set is defined and then orthonormalized by carrying out the Gram−Schmidt procedure. The basis set chosen is given by

$$f(R',\cos\theta';R,\cos\theta) = (R' - R)^n (\cos^2\theta' - \cos^2\theta)^m \tag{9}$$

and the weight function has been defined as

$$w(R',\cos\theta';R,\cos\theta) = \exp\left[-\frac{(R' - R)^2}{2\sigma_R^2} - \frac{(\cos^2\theta' - \cos^2\theta)^2}{2\sigma_\theta^2} \right] \tag{10}$$

The basis set is composed by powers $0 \le n \le 6$ and $0 \le m \le 6$, with the additional condition $n + m \le 6$. Angle θ has been mapped onto cos θ^2 to take implicity into account the symmetry of the potential. Monodimensional fits for each angle have been done to create a regular grid of points in $\mathbf{R}$ in order to have a sufficent number of input data close to the point for which the DAF fit is evaluated. The variances σ_R and σ_θ in the weight function (9) have been taken as the square of the maximum steps along R and $\cos^2\theta$. Given the high number of input points and the fact that eqs 6−7 have to be evaluated for each point, large amounts of computing time have been saved by defining a cutoff region around each point to be fitted: with a Gaussian weight function only a relatively small region around the point $\mathbf{x}$ had to be evaluated to achieve the highest numerical accuracy.

Figure 6 reports the surface obtained by interpolation. Particularly interesting are the barriers in the region between $R = 2.2-4$ Å, for small angles, since they could account for the inelastic scattering. In such case, the total reactive cross section determined from the difference between the total cross section and the inelastic cross section would be a very good estimate.

4. Dynamics: Theory

As we have seen before, several detailed aspects of the reaction between carbon and acetylene can be studied by reducing it to the addition process, i.e., by taking into account only the entrance reaction channel. The inelastic process itself involves too many degrees of freedom to be treated exactly. A reasonable approximation is to treat the vibrational degrees of freedom of acetylene adiabatically, assuming that the vibrational quantum numbers will be conserved in the first step of the reaction and can be described in the harmonic approximation. Thus, the dynamics of the addition process will be determined by the motion on a potential energy surface labeled with the set $\{n\}$ of vibrational quantum numbers of the molecules, $V_{\{n\}}(R,\theta)$. We can assume that the vibrational modes of the molecule will be inaccessible at the scattering energy of the calculations so that only the adiabatic potential corresponding to the ground state of the molecule will be taken into account, so that we can put $V_{\{0\}}(R,\theta) = V(R,\theta)$. Therefore, the Hamiltonian for the addition process, in the body fixed frame[37] with the Z axis along the atom−molecule vector, is given by

$$H = \frac{-\hbar^2}{2\mu R} \frac{\partial^2}{\partial R^2} R + B_e \hat{\mathbf{j}}^2 + \frac{\hbar^2}{2\mu R^2} |\hat{\mathbf{J}} - \hat{\mathbf{j}}|^2 + V(R,\theta) \tag{11}$$

where μ is the reduced mass of the relative motion between the

two particles, **j** is the rotational angular momentum operator of the molecule, **J** is the total angular momentum operator and, R and θ are the coordinates introduced in Figure 1. Another approximation has been made on the rotational constant of the molecule, that has been set to its value at the equilibrium configuration B_e, instead of taking the "adiabatic" value. Given the large number of values of the total angular momentum that contributes to the reaction, the Centrifugal Sudden approximation (CSA)[37,38] has been applied as follows:

$$|\hat{\mathbf{J}} - \hat{\mathbf{j}}|^2 \approx J(J+1) + \hat{\mathbf{j}}^2 - 2\Omega^2 \tag{12}$$

where Ω is the projection of both the molecular and the total angular momentum on the body-fixed Z axis. In the equation above, Coriolis terms that couple states with different Ω have been neglected, therefore the projection quantum number Ω will be conserved.

The final Hamiltonian is equivalent to the Capture Theory (CT) Hamiltonian[39] for the reaction of an atom with a linear molecule: however, in this case the potential $V(R,\theta)$ is a more accurate adiabatic potential instead of the asymptotic interaction usually employed in CT calculations.

The scattering problem has been solved in the framework of time dependent (TD) quantum mechanics by solving the time dependent Schrödinger equation

$$i\hbar \frac{\partial \Psi}{\partial t} = H\Psi \tag{13}$$

that allows us to specify the initial state of the target (the rotational state of the molecule in this case) to calculate reaction probabilities for a range of energies with one calculation and to impose boundary conditions far from the asymptotic region utilizing the flux method.

The Hamiltonian has been evaluated by discrete variable representation (DVR)[40] on a two-dimensional grid given by the direct product of an equally spaced grid of distances R (corresponding to a sine function basis set) and an angular grid in θ, given by Gauss-Legendre quadrature points. Such a basis set allows a very efficient multiplication of the wavevectors by the Hamiltonian matrix. This feature is very important since this operation is repeated several times for each time step in the short iterative Lanczos propagations (SIL)[41,42] employed in this study: therefore, the computational effort basically depends on the efficiency of this matrix multiplication. The matrix elements of the different terms in the Hamiltonian (eq 11) in this DVR basis have been reported previously (see, e.g., refs 43 and 44). The initial wave function is given by the product of a pure rotational state of the molecule and a Gaussian wave packet:

$$\Psi_{j,\Omega}(t=0) = \phi(R) Y_{j,\Omega}(\theta,0) \tag{14}$$

with

$$\phi(R) = \left(\frac{1}{\pi\delta^2}\right)^{(1/4)} \exp\left[-\frac{(R-R_0)^2}{2\delta^2}\right] \exp(-ik_0 R) Y_{j,\Omega}(\theta,0)/R \tag{15}$$

where R_0 is the starting point of the wave packet and δ controls both the diffusion of the wave packet on the coordinate space and the width of the energy distribution. The latter is centered around the value $E_0 = h^2k_0^2/2\mu$. $Y_{j,\Omega}$ is a spherical harmonic describing the initial rotational state of the molecule.

The flux method has been used to calculate reaction and inelastic probabilities. The flux operator $\hat{F}$, across the surface $g(\mathbf{x}) = 0$, can be defined as

$$\hat{F} = \frac{1}{2}\left\{\delta[g(\mathbf{x})]\frac{\partial g}{\partial \mathbf{x}}\hat{\mathbf{D}} + \hat{\mathbf{D}}\delta[g(\mathbf{x})]\frac{\partial g}{\partial \mathbf{x}}\right\} \tag{16}$$

where $\hat{\mathbf{D}}$ is a "velocity" operator and the flux has been written so that the total flux through $g = 0$ can be written as a volume integral.[45] Given the Hamiltonian in eq 11 and the volume element $dV = R^2 \sin\theta d\theta dR d\phi$, from the conservation of the probability density and the Gauss' theorem, the components of the velocity operator along R and θ, D_R and D_θ, are given by

$$D_R = -i\frac{\hbar}{\mu}\frac{\partial}{\partial R} \tag{17}$$

$$D_\theta = -i\left(\frac{2B_e R}{\hbar} + \frac{\hbar}{\mu R}\right)\frac{\partial}{\partial \theta} \tag{18}$$

By using these equations, it is possible to calculate the flux across any arbitrary surface g. The first derivatives necessary for flux calculations are easily implemented when using a DVR basis set, for which analytical first derivatives have been reported.[43,46]

The energy dependence of the flux[47,48] is obtained from the time independent scattering wave function,[48]

$$\Psi_{iE}^{+} = \frac{1}{a(E)}\int_{-\infty}^{+\infty} dt \exp(iEt)\,\Psi_i(t) \tag{19}$$

the square of the coefficient $a(E)$ is the weight of the energy component in the initial wave packet. It is determined from the overlap between the Gaussian wave packet and the asymptotic eigenfunction of the Hamiltonian corresponding to an incoming wave. The coefficient can be efficiently calculated by using the spherical Bessel function $j_l(kR)$ where the integer l is determined by approximating the asymptotic centrifugal term[49] as follows:

$$J(J+1) + j(j+1) - 2\Omega^2 \approx l(l+1) \tag{20}$$

where j is the initial rotational quantum number of the molecule. It has been noted[50] that such a small inaccuracy in the order of the spherical Bessel function leads only to small effect on the S matrix. Furthermore, using a approximate eigenfunction of the asymptotic potential drastically reduces the dimension of the radial grid, allowing to treat large J values almost in the same fashion as $J = 0$. Finally, we have

$$a(E) = \langle \phi(R) | \bar{j}_l(k) \rangle \tag{21}$$

where $\bar{j}$ is obtained from the spherical Bessel of order l by imposing the normalization to the energy. Scattering probabilities as a function of the energy are obtained by[48]

$$P_j^{J,\Omega}(E) = \langle \Psi_{iE}^{+} | \hat{\mathrm{F}} | \Psi_{iE}^{+} \rangle = \sum_f |S_{fj}|^2 \tag{22}$$

where the sum over the final states f runs over the states accessible from the dividing surface. The cross section for the process will be given by

$$\sigma_j(E) = \frac{\pi}{k_j^2(2j+1)} \sum_{J=0} \sum_{\Omega=-\min(J,j)}^{\min(J,j)} (2J+1)\, P_j^{J,\Omega}(E) \tag{23}$$

where k_j is the modulus of the wave vector, given by $k_j = [2\mu(E - E_j)]^{(1/2)}/\hbar$.

After passing the dividing lines, the wave packet is absorbed by a negative imaginary potential, to prevent the reflection from the boundary of the grid. The absorbing potential used in this

study is given by[51]

$$V(x) = -iA \exp\left[-\frac{B}{(x - x^*)}\right] \quad (24)$$

where A and B depend on the energy and the length of the absorbing region and their values have been tabulated.[51]

Since calculations have been carried out for a large number of values of the total angular momentum, different strategies to reduce the computational effort have been applied. The symmetry of the problem reduces the evaluation of angular integrals and matrix elements in the range $[0,\pi/2]$. Furthermore, the reflection symmetry of the radial kinetic energy operator has been also exploited, using the method introduced by Chen and Guo,[52] that allows the calculation of the most expensive term in the Hamiltonian in half of the computing time. Finally, for low J calculations, the dimension of the grid has been drastically reduced by placing the wave packet in a region where inelastic scattering is negligible while the isotropic potential is still so strong to affect the energy distribution $a(E)$.[53] By propagating backward in time, toward very large distances, the correct $a(E)$ distribution can be recovered.

Since time dependent scattering calculations at very low energies are difficult and given that the reaction cross section increases with decreasing energies, rate constants $k(T)$, dependent on the temperature T, could not be calculated using the present approach. Therefore, we have applied the Adiabatic Capture Centrifugal Sudden approximation (ACCSA)[39] where the rotational motion is also treated adiabatically. Starting from the Hamiltonian (eq 11) and imposing the centrifugal sudden approximation as in eq 12, for a fixed value of R, the rotational terms of the Hamiltonian

$$H_{\rm rot} = \mathrm{B_e}\hat{\mathbf{j}}^2 + \frac{\hbar^2}{2\mu R^2}(\hat{\mathbf{j}}^2 - 2\Omega^2) + V(R,\theta) \quad (25)$$

are diagonalized on a basis set of spherical harmonics $Y_{j\Omega}$. The eigenvalues obtained from the diagonalization are rotationally adiabatic curves $\epsilon_{j\Omega}$, that are labeled in order of increasing energy. Including the effect of the centrifugal term of Hamiltonian, the adiabatic curve $V_j^{J\Omega}$ can be generated:

$$V_j^{J\Omega} = \epsilon_{j\Omega} + \frac{\hbar^2}{2\mu R^2} J(J+1) - \mathrm{B_e} j(j+1) \quad (26)$$

The capture theory reaction probability $P_j^{J\Omega}(E)$ is set equal to one when the collision energy E is larger than the maximum value of the potential $V_j^{J\Omega}$, otherwise is zero. The reaction cross section, for the given collision energy and rotational state j, is given by eq 23. The rate constant $k(T)$ is calculated by weighting the cross sections over the Maxwell−Boltzman distribution:

$$k(T) = \left(\frac{8k_{\rm B}T}{\pi\mu}\right)^{1/2} \frac{1}{(k_{\rm B}T)^2} \sum_j \left[(2j+1)\exp\left[-\frac{\mathrm{B_e} j(j+1)}{k_{\rm B}T}\right] \times \int_0^\infty \sigma_j(E) E \exp\left[-\frac{E}{k_{\rm b}T}\right]\right] Q_{\rm rot}(T)^{-1} \quad (27)$$

where $Q_{\rm rot}(T)$ is the rotational partition function and $k_{\rm B}$ is the Boltzmann constant.

5. Results of Calculations

5.1. Reactive Cross Section. In this section, the results of the time dependent calculations will be presented. Reactive cross sections have been obtained by using the potential energy surface for reaction between carbon and acetylene shown in Figure 6 and by using the dynamical method described in the section above.

Flux lines have been put in three different region of the surface: in the asymptotic region (large R distances) and in both microchannels for the reaction, one corresponding to the insertion of the carbon atom in the triple bond of acetylene and the other to a sideways addition. At the first flux line, total reaction probabilities can be obtained from the calculations of the inelastic probabilities and by subtracting the latter to one. Flux lines in the inner regions, followed by an absorbing potential, are placed in potential wells: the flux in a potential well, therefore, gives the probability for the formation of the isomer that has its minimum inside the potential well. As we have discussed before, in our model, the flux for the formation of a C_3H_2 isomer is also taken as the reactive flux for the formation of the C_3H isomer that can be formed from the addition isomer. The sum of the probabilities in the two microchannels gives an alternative way to calculate total reactive probabilities, that can be used to test the convergence on these quantities.

As we have seen in section 3.1, both microchannels lead to the linear C_3H_2. However, the mechanism for the insertion of the carbon atom in the triple bond of acetylene has a saddle point (sp1) at very low distances: if the effect of the centrifugal barrier is taken into account, for large values of the total J the saddle point sp1 will be shifted to energies larger than the collision energy. In such a way, the mechanism for the formation of the linear isomer by insertion will be blocked, and the cyclic C_3H_2 can be formed. This is illustrated schematically in Figure 7, where the minimum energy path for the insertion is shown, together with the centrifugal potential for a high J value. The sum of the two terms gives the effective potential $V_{\rm J}$, that still has a well-defined well for the cyclic isomer while the saddle point sp1 has been shifted to positive energies. For a range of energies of the order of tenths of kelvin, the insertion process is locked for $J \approx 70$.

Time dependent calculations have been carried out for rotational state $j = 0$ of the molecule: given the cold rotational distribution of molecular beams following the supersonic expansion, this value should be representative of the experimental conditions of the molecule. Reaction cross section have been calculated in the energy range 5−70 kJ mol^{-1}, on a radial grid composed by 400 points at low J values, 500 points for larger J, starting from 0 Å with a stepsize of 0.01 Å. The angular grid is composed of 81 Gauss-Legendre quadrature points. The time step used in the propagation is 1.2×10^{-4} fs, with the Hamiltonian expanded on 60 functions in the SIL propagation: those two parameters have been chosen to optimize the computing time and ensure the conservation of the total energy of the wave packet. The flux line in the insertion pathway has been put at $R = 1$ Å when calculating the formation of the linear isomer, while for the cyclic structure it has been put at $R = 1.5$ Å. The second flux line, for the sideways addition, is composed of two segments: the first, in the potential valley, is put at $\theta = 24^0$, for $R \leq 2$ Å while the second segment (measuring the tunneling through the barrier) is put at $R = 2$ Å for $\theta \leq 24^0$. A two-dimensional absorbing potential is needed in the latter case: it has been obtained by smoothing the θ dependent potential (given by eq 24) with a linear function of R (located in a narrow strip around $R = 2$ Å where assumes values between 0 and 1). Calculations have been carried out in the range of total angular momenta between 0 and 125, with a

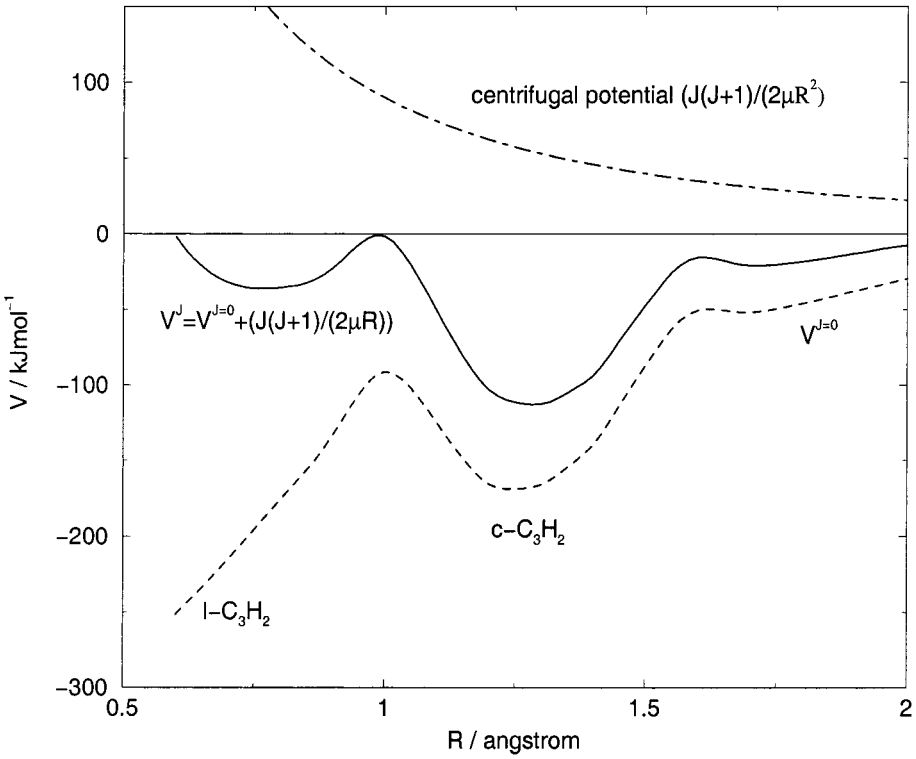

Figure 7. Qualitative picture of the effect of the centrifugal potential: the dashed line is obtained from a cut at fixed angle from the ab initio PES, the dotted−dashed is the centrifugal potential for $J = 50$, and the solid line is the sum of the two potentials.

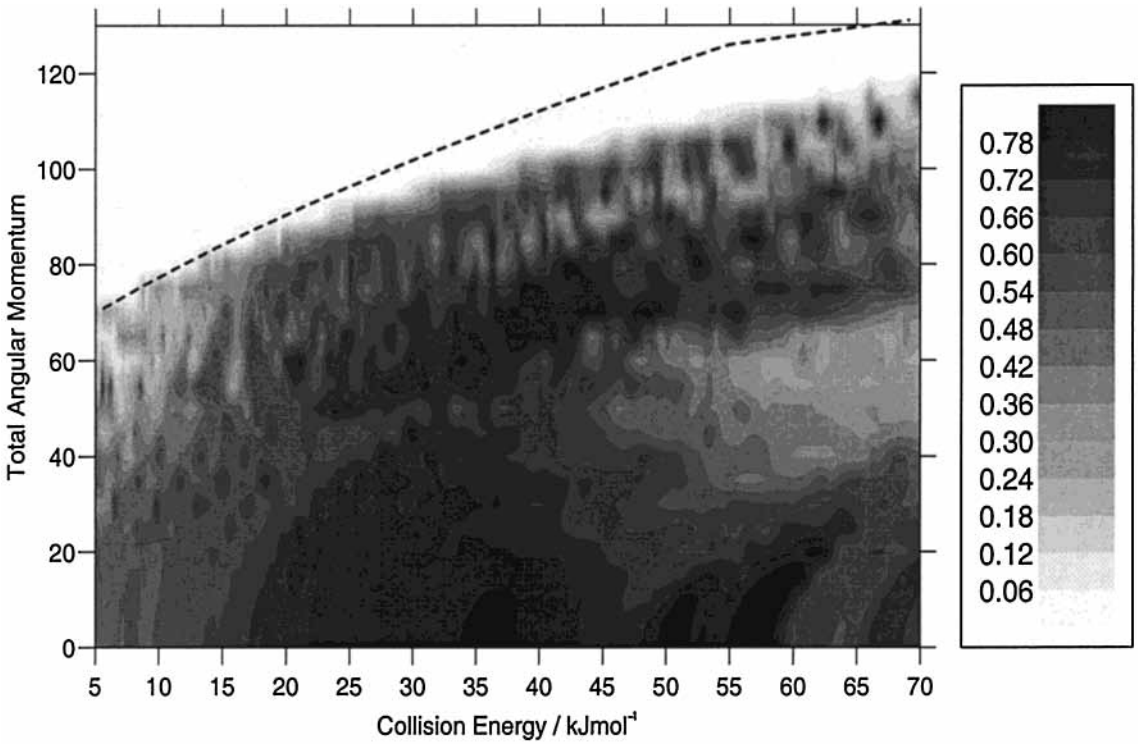

Figure 8. Total reaction probability as a function of the total angular momentum and collision energy (in kJ mol^{-1}). The dashed line represents the limiting J value as a function of the energy calculated by ACCSA, using the ab initio potential.

step $\Delta_J = 5$. The starting point of the wave packet has been located at $R = 6.8$ Å for low J values, $R = 8.8$ Å for higher J.

Results for the reaction probabilities are shown in Figure 8, reported as a function of the total angular momentum J and the collision energies. Values of probabilities range from 0 to 0.8, oscillating both with varying the total angular momentum and the energy in such a way that simple patterns like those suggested by the J shifting approximation[54] (recently extended to reaction without a transition state[53]) are not present. The dashed line reported on the figure is the maximum J_{max}^{ACCSA} that contributes to the ACCSA cross section $\sigma_{j=0}$, calculated from the rotational adiabatic curve $\epsilon_{0,0}$ obtained from the rotational Hamiltonian with the ab initio potential. For capture approximations, the reaction probabilities below that curve (for $J \leq$

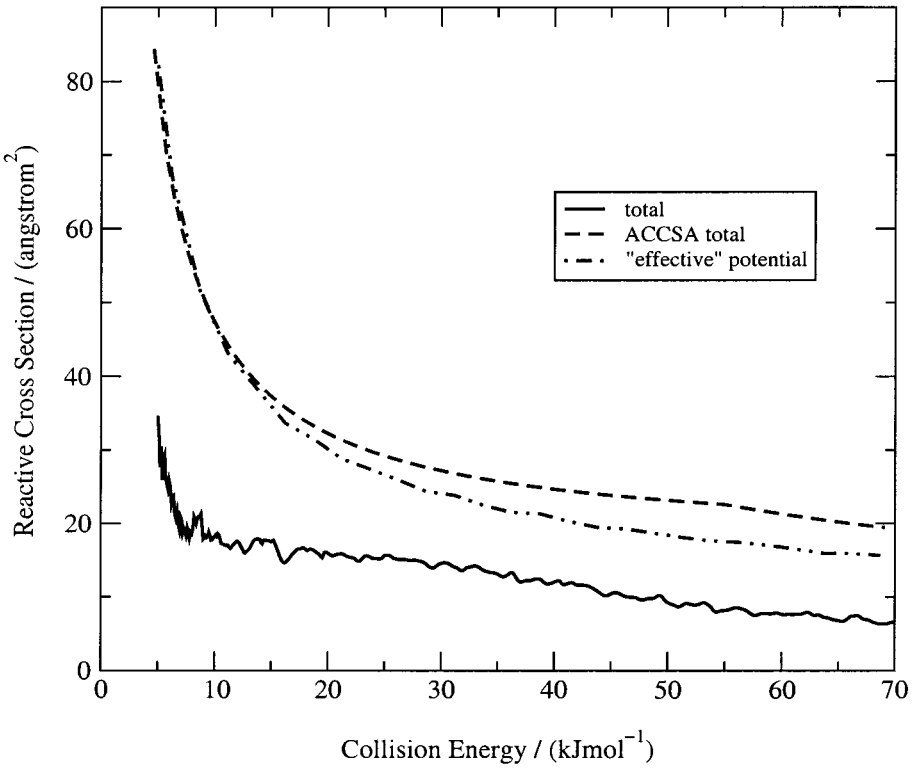

Figure 9. Total reaction cross sections (in Å^2) as a function of the energy (in kJ mol^{-1}), obtained from exact two-dimensional dynamics (solid line), ACCSA (dashed line), and capture approximation on the calculated probabilities in Figure 8 (dotted-dashed line)

J_{max}^{ACCSA}) are equal to one. From the present study, we can see two kind of discrepancies: the first is in the behavior of the reaction probabilities that, apart from being a complicated function of J and E, can also assume rather small values, far from the unity assumed by the capture approximation. The second disagreement is in the prediction of the total angular momenta that contribute to the reaction cross section. The difference between the ACCSA curve J_{max} and the boundary (at high J) of the region where reaction probabilities are different from zero in Figure 8, shows that the number of total angular momenta contributing to the cross section is larger for the ACCSA calculations, in the high energy limit, and goes on the boundary at lower energies. An explanation for this behavior could be in the breakdown of the rotational adiabatic approximation, since the curve $\epsilon_{0,0}$ is the lowest adiabatic curve (therefore, it has the largest number of total momenta J contributing to the cross section) and that adiabatic approximations are valid at low energies. According to Figure 8, for $E < 15$ kJ mol^{-1} the adiabatic approximation should be valid.

The total reaction cross section for the rotational state $j = 0$ of the molecule obtained in the present study is reported in Figure 9, calculated in the energy range 5−70 kJ mol^{-1}. The other two curves reported in the figure are the ACCSA cross section ($j = 0$) and the cross section calculated by setting the probability equal to one for J below the curve limiting the reaction probabilities different from zero, in Figure 8. The resulting cross section corresponds to the application of the capture approximation on an effective potential that includes the contributions of rotational nonadiabatic transitions to other adiabatic curves $\epsilon_{j,\Omega}$ The cross sections obtained from dynamical calculations is roughly half of the ACCSA cross sections on the whole range of energies considered in the calculations: with this respect, the breakdown of the rotational adiabatic approximation does not seem to introduce additional differences between the two cross sections. In this range of energies, therefore, the ACCSA approximation gives qualitative results, with the additional feature of providing a theoretical upper limit to the real cross section.

The results of the application of the model introduced in section 4 are presented in Figure 10, where the total cross section is shown again, this time in comparison with the estimated cross section for the formation of the linear and the cyclic C_3H isomers. It is possible to see more clearly that total and linear cross sections have several small peaks superimposed on the quite regular decreasing behavior. Given the complicated topology of the PES used in the calculation (Figure 6), it seems reasonable to consider those peaks as broad resonant structures. It is worth noting that variational RRKM calculations[17] give an estimated lifetime 10 times larger than the rotational period of the linear C_3H_2 adduct at room temperature, suggesting the possibilty for the reaction to behave statistically. However, the observed angular distributions of the products[11] are not in agreement with this suggestion. Furthermore, Figure 10 shows that the cross section for the formation of the cyclic C_3H is much smaller that the cross section for the linear isomer, with the former that increases with energy to reach an almost constant value at the highest energy of the calculations. The formation of the linear isomer, instead, is the dominant process at the lowest energy of the calculations. As we have discussed before, the formation of the linear isomer can follow two different mechanisms: the insertion to the C−C bond of acetylene (at low angular momenta J) and the sideways addition. Figure 11 reports the contributions due to the two pathways for the formation of the linear isomer: the sideways addition (path 2) gives a slightly decreasing cross section while the addition to the C−C bond (path 1) is a process fastly decreasing with the energy. The behavior of the latter is due to the fact that a limited number of total angular momenta (or, alternatively, of impact parameters) contribute to the cross

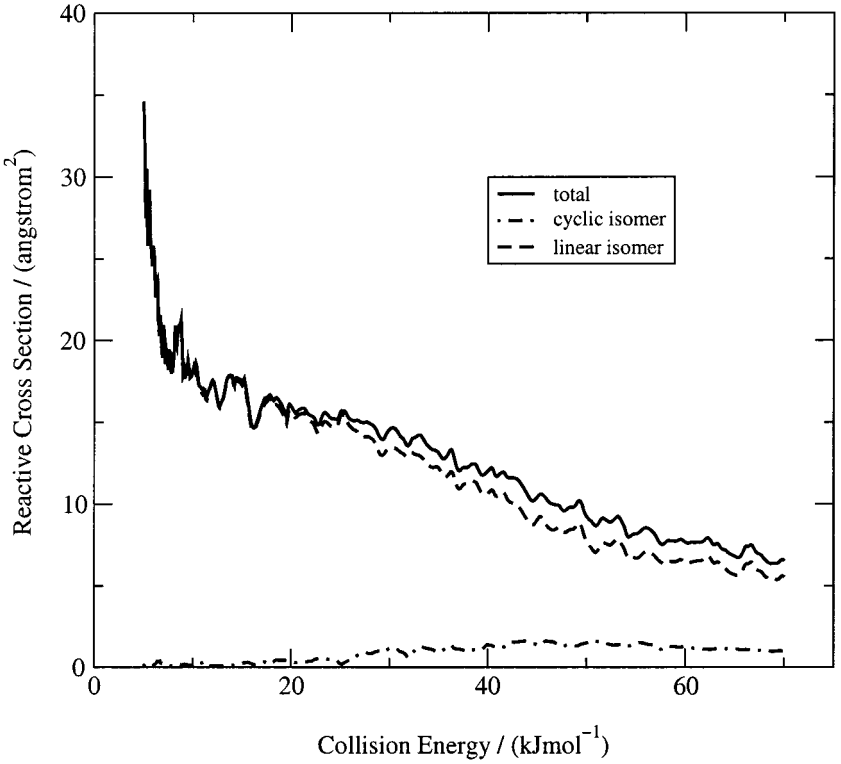

Figure 10. Reactive cross sections (in Å^2) as a function of the collision energy (in kJ mol^{-1}) obtained from exact two-dimensional calculations and application of the model in section 2: total cross section (solid line), cyclic C_3H formation cross section (dotted−dashed line), and linear C_3H formation cross section (dashed line).

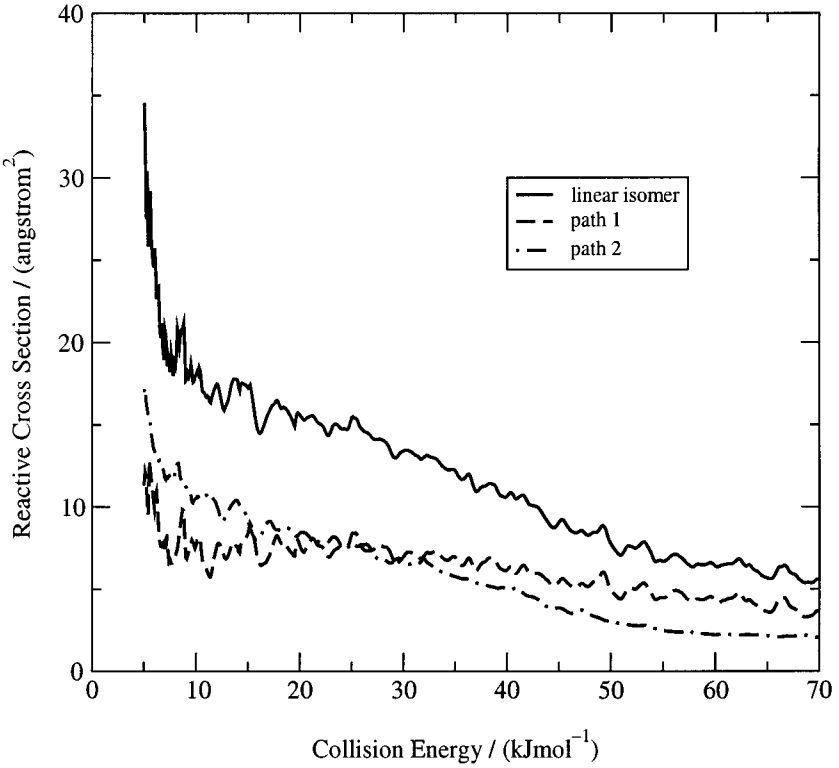

Figure 11. Reactive cross section (in Å^2) for the formation of the linear C_3H, as a function of the energy (in kJ mol^{-1}): the contribution of the sideways addition (path 1, dashed line) and of the insertion (path 2, dotted−dashed line) are shown, together with the solid cross section for the formation of the linear isomer (solid line).

section because of the shift of the saddle point sp1 with increasing J (see Figure 7).

Finally, Figure 12 report the calculated branching ratio for the formation of the cyclic and linear C_3H: as we have seen from Figure 10, the linear isomer is the dominant product of the reaction. From this figure, we can see that the cyclic C_3H is a negligible fraction of the product for energies less that 20 kJ mol^{-1}, after which it increases to reach approximately the 18% of the linear isomer. Therefore, the model we have applied to the reaction suggests that the cyclic C_3H is only formed at

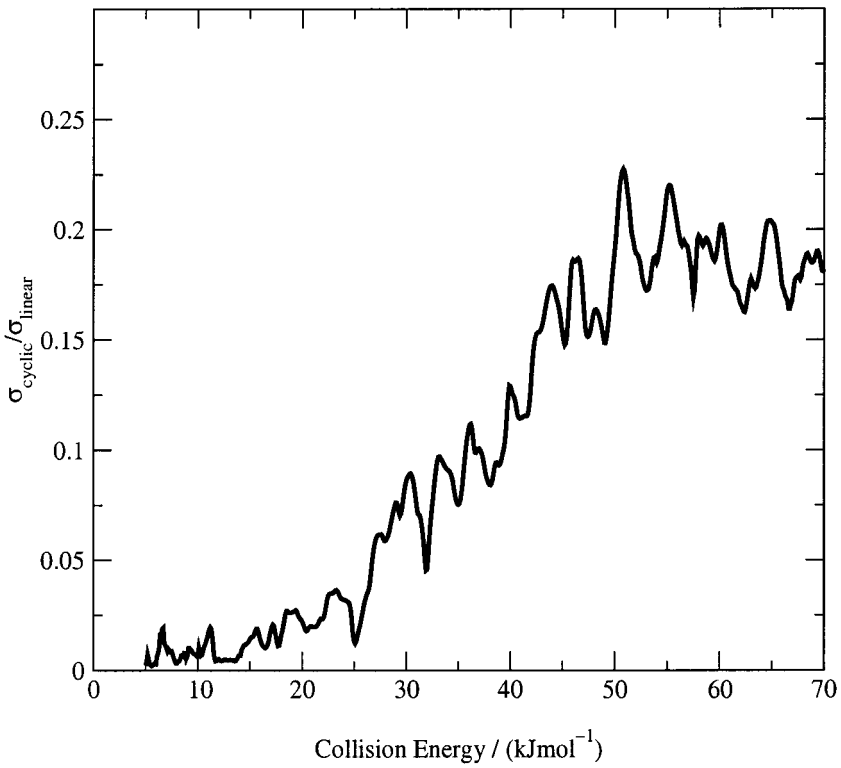

Figure 12. Branching ratio for the formation of the cyclic and linear C_3H, as a function of the energy (in kJ mol^{-1}).

rather high energies and in smaller quantities with respect to the linear isomer. The latter is almost the exclusive product at low energies. This result contradicts the interpretation of the molecular beam experiments,[11] discussed in section 2, that identified the cyclic C_3H as the product formed at the lowest energies, since the existence of the insertion path, mainly responsible for the outcome of the calculations, has been excluded in rationalizing the experimental results[11] However, the present results are not able to explain the results of the molecular beam experiments since the predominance of the linear C_3H at low energies would bring to a backward−forward symmetry in the angular distribution of the product, due to the C_2 symmetry of propargylene (l-C_3H_2), while, at higher energies, the formation of a significant fraction of cyclic C_3H would lead to a nonsymmetrical angular distribution, since the corresponding intermediate (c-C_3H_2) has no symmetry. Therefore, additional theoretical and experimental work is needed to understand the products of the reactions.

5.2. Rate Constants. As we have mentioned before, time dependent calculations could not be extended to very low energies, since they are technically very difficult in that energy range. Therefore, rate constants for the reaction at low temperature have been calculated by applying the adiabatic capture centrifugal sudden approximation (ACCSA), using the ab initio potential described in section 3.

The results of the calculations are reported in Figure 13: the dotted curve is the ACCSA rate constant, showing a rather good agreement with the fitting of the experimental rate constants[9]-(full curve), taking into account a ±20% error on the experimental curve. In particular, the slight negative temperature dependence of the rate constant is very well reproduced by the calculations. It is worth noting that this kind of agreement comes from the use of a more realistic PES: the dashed curve is the ACCSA rate constant calculated by using the asymptotic potential given by eq 1. As we can see from the figure, this potential leads to a rate constant with a weak positive dependence on the temperature. Finally, since we have found from

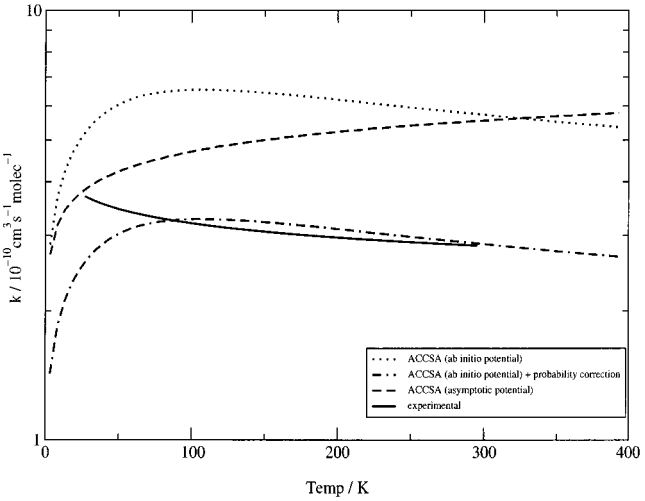

Figure 13. Reaction rate constans as a function of the temperature: the experimental results[9] (solid line) are compared with the ACCSA calculations using the ab initio potential (dotted line) and the long-range interaction (dashed line). Rate constants obtained from ACCSA calculations on the ab initio potential after applying a probability factor (dot−dashed line), obtained from results in Figure 9.

the cross section calculations discussed above that the capture approximation is not valid for a rather large range of energies, we have calculated a correction to the ACCSA rate constant assuming a reaction probability of 0.5 instead of one. This value represents, approximately, the ratio between capture cross section and the cross section calculated with the dynamical method discussed in section 4. The dot−dashed curve in Figure 13 is the corrected version of ACCSA rate constant, which has a quite good agreement with the experimental fitting over a large range of temperature.

It is interesting to understand the difference between ACCSA calculations done on the *ab inito* PES and those that use the asymptotic interaction: Figure 14 shows some rotational

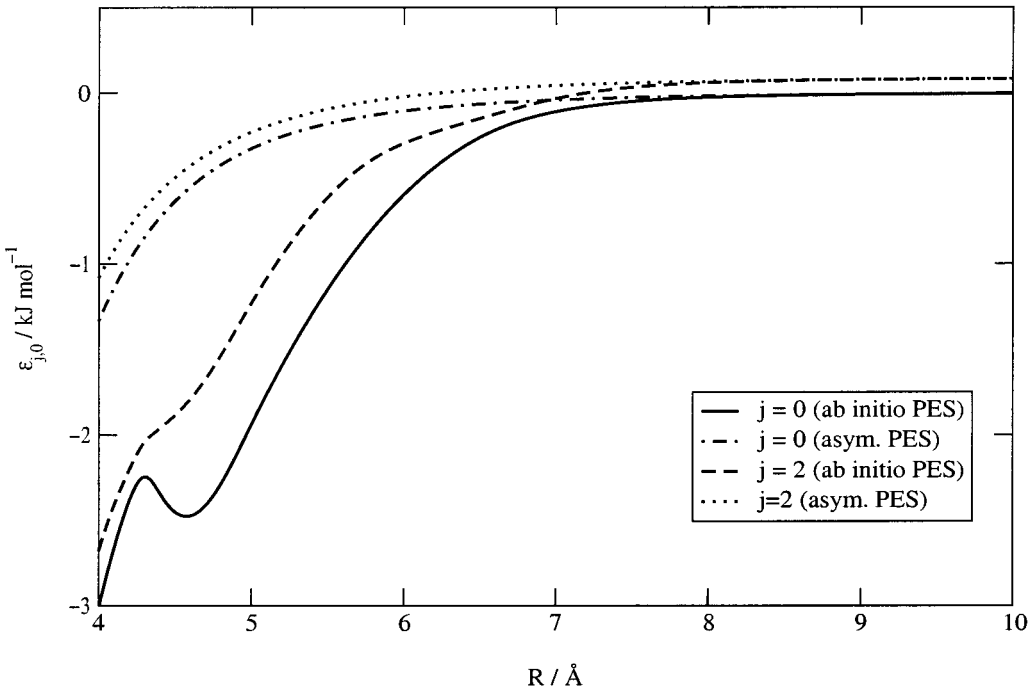

Figure 14. Rotational adiabatic curves (in kJ mol^{-1}) as a function of the distance (in Å), for rotational states $j = 0$ and 2, calculated from the ab initio PES and the long-range interaction.

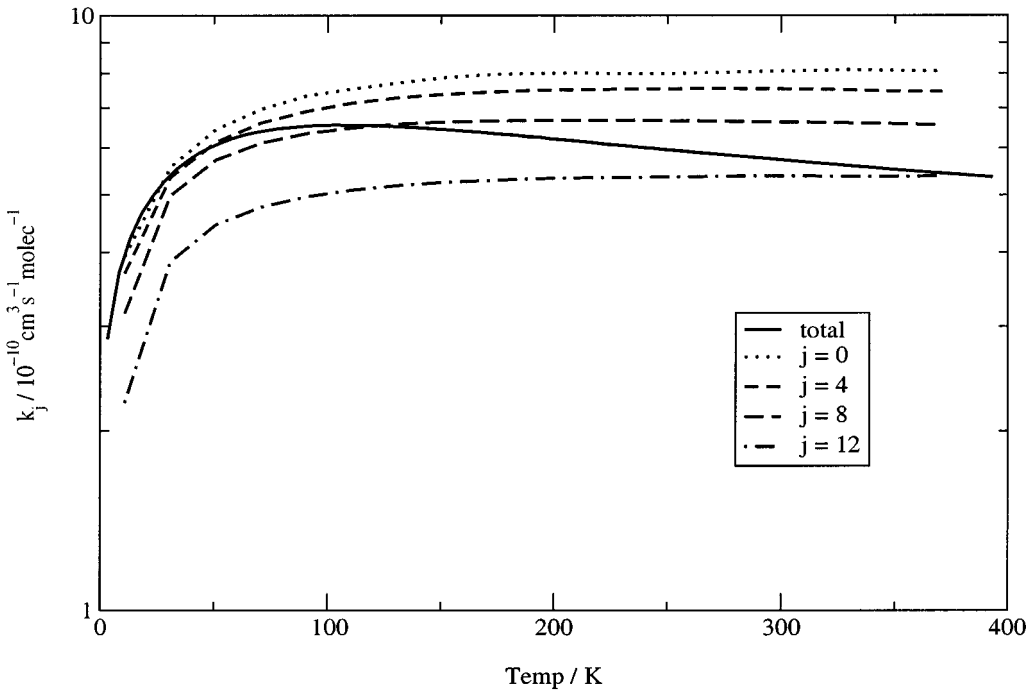

Figure 15. ACCSA rate constants for the initial rotational state j as a function of the temperature, calculated from the ab initio potential, reported for $j = 0$, 4, 8, 12. The total (statistically weighted) rate constant is also shown (solid line).

adiabatic curves calculated for both potentials, for two values of j. Marked differences between the same adiabatic curve of different potentials exists for $R \leq 8$. We could also note that, in the radial range shown in the figure, the adiabatic curves calculated from the asymptotic potential have the same shape while the rotational adiabatic curves of the ab inito potential are quite different between them.

Such differences are reflected in the state selected rate constant $k_j(T)$ reported in Figure 15: the differences among them are more marked with respect to those reported for the asymptotic potential.[16] We can also note that the state selected rate constants increase with the temperature over the whole range of T: therefore, the negative temperature dependence is due to the change in the statistical weight of the initial rotational state. Such effect has also been found theoretically for the reaction between SO + OH.[55]

6. Conclusions

The reaction between C(^{3}P) and acetylene, in its electronic ground state, has been studied by a reduced dimensionality model restricted to the entrance channel, on the lowest triplet state. A potential energy surface has been calculated by using the CCSD(T) method, as a function of two variables describing the position of the carbon atom with respect to acetylene.

Calculations of the total reactive cross section have been done in the energy range between 5 and 70 kJ mol^{-1}, showing that this quantity has a qualitative trend that is consistent with the capture theory predictions. However, the detailed features of the cross sections depends both on the contribution of the inelastic processes and on the presence of several potential wells in the interaction, producing broad resonance peaks. A model for the formation of the linear and cyclic C_3H has been developed, that restricts the study of the reaction to the addition process, i.e., to the formation of the linear and cyclic isomers of the stable intermediates C_3H_2, producing the linear and cyclic C_3H isomers. It is found that the linear C_3H is formed preferentially, over the whole range of energies considered in the present study. The cyclic isomer of C_3H, instead, has an appreciable formation probability at the highest energies and gives a very small contribution at the lowest energies. This result contradicts an interpretation of the molecular beam experiments.[11] Clearly, additional theoretical and experimental studies are needed to understand the products of the reaction.

Rate constants have also been calculated by applying the ACCSA approximation on the CCSD(T) potential energy surface. Results have shown a good agreement with those obtained in recent experiments,[9] showing that ACCSA can produce quite reliable results when employed with a more accurate potential with respect to the usual asymptotic interaction used in capture theory studies.

Acknowledgment. This was supported by the TMR network of the European Union on Astrophysical Chemistry and by the Engineering and Physical Science Research Council.

References and Notes

(1) Bettens, R. P. A.; Lee, H.-H.; Herbst, E. *Astrophys. J.* **1995**, *443*, 664.
(2) Herbst, E. *Annu. Rev. Phys. Chem.* **1995**, *46*, 27.
(3) Williams, D. A. *Contemp. Phys.* **1994**, *35*, 269.
(4) Lequeux, J.; Roueff, E. *Phys. Rep.* **1991**, *200*, 241.
(5) Clary, D. C.; Haider, N.; Husain, D.; Kabir, M. *Astrophys. J.* **1994**, *422*, 416.
(6) Sims, I. R.; Smith, I. W. M. *Annu. Rev. Phys. Chem.* **1995**, *46*, 109.
(7) Smith, I. W. M.; Rowe, R. R. *Acc. Chem. Res.* **2000**, *33*, 261.
(8) Terzieva, R. V.; Herbst, E. *Faraday Discuss.* **1998**, *109*, 250.
(9) Chastaing, D.; James, P. L.; Sims, I. R.; Smith, I. W. M. *Faraday Discuss.* **1998**, *109*, 247. Chastaing, D.; James, P. L.; Sims, I. R.; Smith, I. W. M. *Phys. Chem. Chem. Phys.* **1999**, *1*, 2247.
(10) Bettens, R. P. A.; Herbst, E. *Astrophys. J.* **1997**, *478*, 585.
(11) Kaiser, R. I.; Ochsenfeld, C.; Head-Gordon, M.; Lee, Y. T.; Suits, A. G. *J. Chem Phys* **1997**, *106*, 1729. Kaiser, R. I.; Ochsenfeld, C.; Head-Gordon, M.; Lee, Y. T.; Suits, A. G. *Science* **1996**, *274*, 1508.
(12) Kaiser, R. I.; Lee Y. T.; Suits, A. G. *J. Chem. Phys.* **1996**, *105*, 8705. Kaiser, R. I.; Stranges, D.; Lee Y. T.; Suits, A. G. *J. Chem. Phys.* **1996**, *105*, 8721. Kaiser, R. I.; Stranges, D.; Bevsek, H. M.; Lee Y. T.; Suits, A. G. *J. Chem. Phys.* **1997**, *106*, 4945. Kaiser, R. I.; Sun, W.; Suits, A. G.; Lee, Y. T. *J. Chem. Phys.* **1997**, *107*, 8713. Kaiser, R. I.; Hahndorf, I.; Huang, L. C. L.; Lee, Y. T.; Bettinger, H. F.; Schleyer, P. v. R.; Schaefer III, H. F.; Schreiner, P. R. *J. Chem. Phys* **1999**, *110*, 6091. Kaiser, R. I.; Mebel, A. M.; Chang, A. H. H.; Lin, S. H.; Lee, Y. T. *J. Chem. Phys.* **1999**, *110*, 10330.
(13) Ochsenfeld, C.; Kaiser, R. I.; Lee, Y. T.; Suits, A. G.; Head-Gordon, M. *J. Chem. Phys.* **1997**, *106*, 4141.
(14) Bettinger, H. F.; Schleyer, P. v. R.; Schaefer, H. F., III; Schreiner, P. R.; Kaiser, R. I.; Lee, Y. T. *J. Chem. Phys* **2000**, *113*, 4250.
(15) Scholefield, M. R.; Choi, J.-H.; Goyal, S.; Reisler, H. *Chem. Phys. Lett.* **1998**, *288*, 487.
(16) Liao, Q.; Herbst, E. *Astrophys. J.* **1995**, *444*, 694.
(17) Guadagnini, R.; Schatz, G. C.; Walch, S. P. *J. Phys. Chem. A* **1998**, *102*, 5857.
(18) Takahashi, J.; Yamashita, K. *J. Chem. Phys* **1996**, *104*, 6613.
(19) Seburg, R. A.; Patterson, E. V.; Stanton, J. F.; McMahon, R. J. *J. Am. Chem. Soc.* **1997**, *119*, 5847.
(20) Mebel, A. M.; Jackson, W. M.; Chang, A. H. H.; Lin, S. H. *J. Am. Chem. Soc.* **1998**, *120*, 5751.
(21) Jonas, V.; Böhme, M.; Frenking, G. *J. Phys. Chem.* **1992**, *96*, 1640.
(22) Vereecken, L.; Pierloot, K.; Peeters, J. *J. Chem. Phys.* **1998**, *108*, 1068.
(23) Herges, R.; Mebel, A. M. *J. Am. Chem. Soc.* **1994**, *116*, 8229.
(24) Maier, G.; Reisenauer, H. P.; Schwab, W.; Čársky, P.; Hess, B. A., Jr.; Schaad, L. J. *J. Am. Chem. Soc.* **1987**, *109*, 5183.
(25) Song, X.; Bao, Y.; Urdahl, R. S.; Gosine, J. N.; Jackson, W. M. *Chem. Phys. Lett.* **1994**, *217*, 216.
(26) Frisch, M. J.; Trucks, G. W.; Schlegel, H. B.; Scuseria, G. E.; Robb, M. A.; Cheeseman, J. R.; Zakrzewski, V. G.; Montgomery Jr, J. A.; Stratmann, R. E.; Burant, J. C.; Dapprich, S.; Millam, J. M.; Daniels, A. D.; Kudin, K. N.; Strain, M. C.; Farkas, O.; Tomasi, J.; Barone, V.; Cossi, M.; Cammi, R.; Mennucci, B.; Pomelli, C.; Adamo, C.; Clifford, S.; Ochterski, J.; Petersson, G. A.; Ayala, P. Y.; Cui, Q.; Morokuma, K.; Malick, D. K.; Rabuck, A. D.; Raghavachari, K.; Foresman, J. B.; Cioslowski, J.; Ortiz, J. V.; Stefanov, B. B.; Liu, G.; Liashenko, A.; Piskorz, P.; Komaromi, I.; Gomperts, R.; Martin, R. L.; Fox, D. J.; Keith, T.; Al-Laham, M. A.; Peng, C. Y.; Nanayakkara, A.; Gonzalez, C.; Challacombe, M.; Gill, P. M. W.; Johnson, B. G.; Chen, W.; Wong, M. W.; Andres, J. L.; Head-Gordon, M.; Replogle, E. S.; Pople, J. A. *Gaussian 98*, Revision A.3; Gaussian, Inc.: Pittsburgh, PA, 1998.
(27) Raghavachari, K.; Trucks, G. W.; Pople, J. A.; Head-Gordon, M. *Chem. Phys. Lett.* **1989**, *157*, 479.
(28) Dunning, T. H. *J. Chem. Phys.* **1989**, *90*, 1007.
(29) Seburg, A.; McMahon, R. J. *Angew. Chem.* **1995**, *107*, 2198.
(30) Knowles, P. J.; Hampel, C.; Werner, H. J. *J. Chem. Phys.* **1993**, *99*, 5219. Triple excitation as in Watts, J. D.; Gauss, J.; Bartlett, R. J. *J. Chem. Phys.* **1993**, *98*, 8718.
(31) It has been reported recently (Knowles, P. J.; Hampel, C.; Werner, H.-J. *J. Chem. Phys.* **2000**, *112*, 3106) that some formulas implemented in the Molpro version we have used in the present study are incomplete. The inclusion of the additional terms gives an estimated contribution smaller than 10^{-4} hartree to the electronic energy. To evaluated how this error affects our calculations, we have carried out unrestricted coupled cluster calculations (UCCSD(T)), implemented in Molpro, on the stationary points of C_3H_2. Results on test systems, reported in the paper mentioned above, give differences of 10^{-3} hartree between UCCSD(T) and uncorrected RCCSD-(T) results: the same order of magnitude has been found on the present system. Furthermore, the differences on the interaction energies between UCCSD(T) and RCCSD(T) results are of the order of few kJ mol^{-1}. We can therefore assume that the effect of the correction is negligible on the present system.
(32) Werner, H.-J.; Knowles, P. J.; Almlöf, J.; Amos, R. D.; Berning, A.; Cooper, D. L.; Deegan, M. J. O.; Dobbyn, A. J.; Eckert, F.; Elbert, S. T.; Hampel, C.; Lindh, R.; Lloyd, A. W.; Meyer, W.; Nicklass, A.; Peterson, K. A.; Pitzer, R. M.; Stone, A. J.; Taylor, P. R.; Mura, M. E.; Pulay, P.; Schütz, M.; Stoll, H.; Thorsteinsson, T. MOLPRO Quantum Chemistry Package, version 96.4, 1996.
(33) Hirschfelder, J. O.; Curtiss, C. F.; Bird, R. B. *Molecular Theory of Gas and Liquid*; Wiley: New York, 1954.
(34) Halberstadt, N. In *Fitting Molecular Potential Energy Surfaces*; Law, M. M., Hutson, J. M., Ernesti, A., Eds.; CCP6: Daresbury, 1993.
(35) Hoffman, D. K.; Marchioro II, T. L.; Arnold, M.; Huang, Y.; Zhu, W.; Kouri, D. J. *J. Math. Chem.* **1996**, *20*, 117.
(36) Frishman, A.; Hoffman, D. K.; Kouri, D. J. *J. Chem. Phys.* **1997**, *107*, 804.
(37) Pack, R. T. *J. Chem. Phys.* **1974**, *60*, 633.
(38) McGuire, P.; Kouri, D. J. *J. Chem. Phys.* **1974**, *60*, 2488.
(39) Clary, D. C. *Mol. Phys.* **1985**, *54*, 605.
(40) Light, J. C.; Hamilton, I. P.; Lill, J. V. *J. Chem. Phys.* **1985**, *82*, 1400.
(41) Park, T. J.; Light, J. C. *J. Chem. Phys.* **1986**, *85*, 5870.
(42) Leforestier, C.; Bisseling, R. H.; Cerjan, C.; Feit, M. D.; Friesner, R.; Guldberg, A.; Hammerich, A.; Jolicard, G.; Karrlein, W.; Meyer, H.-D.; Lipkin, N.; Roncero, O.; Kosloff, R. *J. Comput. Phys.* **1991**, *94*, 59.
(43) Colbert, D. T.; Miller, W. H. *J. Chem. Phys.* **1992**, *96*, 1982.
(44) Aguado, A.; Paniagua, M.; Lara, M.; Roncero, O. *J. Chem. Phys* **1997**, *107*, 10085.
(45) Miller, W. H. *J. Chem. Phys.* **1974**, *61*, 1823.
(46) Szalay, V. *J. Chem. Phys.* **1993**, *99*, 1978.
(47) Neuhauser, D. *Chem. Phys. Lett.* **1992**, *200*, 173.
(48) Zhang, D. H.; Zhang, J. Z. H. *J. Chem. Phys.* **1994**, *101*, 3671.
(49) de Lara, M. P.; Villarreal, P.; Delgado- Barrio, G.; Miret-Artès, S.; Buonomo, E.; Gianturco, F. A. *Chem. Phys. Lett.* **1995**, *242*, 336.
(50) Walker, R. B.; Hayes, E. P. In *The Theory of Chemical Reaction Dynamics*; Clary, D. C., Ed.; Reidel: Dordrecht, 1986; p 105.
(51) Vibok, Á.; Balint-Kurti, G. G. *J. Phys. Chem.* **1992**, *96*, 8712.
(52) Chen, R.; Guo, H. J. *Chem. Phys* **1999**, *110*, 2771.
(53) Gray, S. K.; Goldfield, E. M.; Schatz, G. C.; Balint-Kurti, G. G. *Phys. Chem. Chem. Phys.* **1999**, *1*, 1141.
(54) Bowman, J. M. *J. Phys. Chem.* **1991**, *95*, 4960.
(55) Clary, D. C. *Annu. Rev. Phys. Chem.* **1990**, *41*, 61.